JOURNAL OF MAGNETIC RESONANCE **135,** 406–417 (1998)
ARTICLE NO. MN981568

Matrix Line in Pulsed Electron-Nuclear Double Resonance Spectra

Andrei V. Astashkin*,[1] and Asako Kawamori†

*The Institute of Chemical Kinetics and Combustion, Russian Academy of Sciences, 630090 Novosibirsk, Russia; and †Faculty of Science, Kwansei Gakuin University, Uegahara 1-1-155, Nishinomiya 662, Japan

Received January 7, 1998; revised July 23, 1998

The intense line in Mims and Davies electron-nuclear double resonance (ENDOR) spectra due to the hyperfine interactions of an unpaired electron with distant matrix nuclei is shown to originate from a simultaneous inversion of a large number of nuclear spins by a radiofrequency pulse. Theoretical expressions describing the matrix ENDOR effect are derived and verified experimentally.

Key Words: **ESE; pulsed ENDOR; Mims ENDOR; Davies ENDOR; matrix line.**

INTRODUCTION

There are two basic techniques of pulsed electron-nuclear double resonance (ENDOR) spectroscopy, one due to Mims (*1*) and the other due to Davies (*2*), that are used most often in practical applications. Both techniques have been described in detail in several theoretical (*3, 4*) and review works (*5–8*). Their common feature is that the ENDOR effect, according to the available theory, becomes smaller for smaller hyperfine interaction (hfi) constants. Nevertheless, in the ENDOR spectra obtained by both methods, quite frequently, the most intense line is that due to the distant matrix protons, that is, nuclei with extremely small hfi (for the examples see (*5–13*)). To our knowledge, so far no satisfactory explanation of this fact has been given in the literature and the above theoretical and review works (*3–8*) do not discuss this matter in detail. An analysis given in this work allows one to reconcile the high intensity of the matrix line with the mentioned property of the Mims and Davies ENDOR techniques consisting in the decrease of the ENDOR response with decreasing hfi constant.

EXPERIMENTAL

The pulsed ENDOR measurements were performed on a pulsed EPR spectrometer ESP-380 (Bruker) equipped with a cylindrical dielectric ENDOR cavity (EN4118X-MD5, Bruker) and a cryogenic gas flow system. The radiofrequency (RF) pulse was supplied through the 500-W amplifier (ENI model 500A). The durations of the 90° microwave (mw) pulses in the Mims ENDOR experiment were 16 ns. The measurement temperature was 80 K.

In the Davies ENDOR measurement, the duration of the first (180°) mw pulse was 800 ns. The detection sequence consisted of two non-selective 90° and 180° mw pulses with the durations of 16 and 24 ns, respectively. The measurement temperature was 30 K.

RESULTS AND DISCUSSION

1. General Assumptions and Approach to the Analysis

We will assume an unpaired electron with a spin $S = \frac{1}{2}$ to interact with nuclei of spin $I = \frac{1}{2}$, which corresponds to the most practical case of proton ENDOR. The static magnetic field $\mathbf{B_o}$ is assumed to be parallel to the Z-axis of a laboratory frame and the Hamiltonian of the spin system is taken in the form

$$\hat{H} = \nu_e \hat{S}_Z - \nu_I \hat{I}_Z + A\hat{S}_Z\hat{I}_Z, \qquad [1]$$

where $\nu_e = g_e\beta_e B_o/h$ (g_e is an electron g-factor and β_e is Bohr magneton) is a Larmor frequency of the electron in the applied magnetic field, $\nu_I = g_N\beta_N B_o/h$ (g_N is a nuclear g-factor and β_N is a nuclear magneton) is a nuclear Zeeman frequency, and A is a secular part of hfi,

$$A = a_{iso} + D. \qquad [2]$$

In the last expression a_{iso} is an isotropic hfi constant and D is an electron-nuclear dipole interaction (anisotropic hfi). In the point dipole approximation that we will use for distant matrix nuclei, the dependence of D on the distance R between the unpaired electron and a nucleus and on the angle θ between $\mathbf{B_o}$ and $\mathbf{R}$ is given by

$$D = D_o[1 - 3\cos^2\theta] \qquad [3]$$

with

$$D_o = g_e g_N \beta_e \beta_N / hR^3. \qquad [4]$$

[1] Visiting professor of Kwansei Gakuin University. Current address: University of Arizona, Department of Chemistry, Tucson, AZ 85721. Corresponding author. E-mail: andrei@u.arizona.edu.

1090-7807/98 $25.00

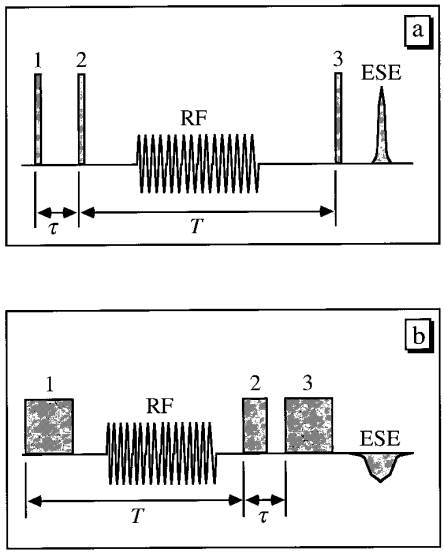

FIG. 1. The pulse sequences of Mims (a) and Davies (b) ENDOR.

All non-secular terms in Eq. [1] are neglected. This represents a fair approximation for a usual situation of $|D_o| < |2\nu_I \pm A|$ and $|A| \ll |\nu_e|$.

Our analysis will take into account the interaction of the unpaired electron with many equivalent nuclei simultaneously. Therefore, we could start our consideration of the Mims ENDOR effect directly from the analytical expression derived for such a situation by Liao and Hartmann (*3*). However, we have found it beneficial to use a classical model considering an effect of the local magnetic field produced by the nuclear spins on the precession of the electron spin and a resonance frequency of its transitions. Under our assumption about the absence of non-secular terms in the spin-Hamiltonian (Eq. [1]) this simple approach is as rigorous as the density matrix one used in (*3*) (and leads, of course, to the same results), but it seems to be more transparent for the qualitative understanding of the physics of the phenomena.

Throughout the discussion, the electron spin relaxation is considered to be independent of the RF-induced changes in a nuclear spin system and is not taken into account explicitly. Thus, the ESE signals are always assumed to be normalized by the relaxation decay.

2. The Origin and General Properties of Mims ENDOR Effect

The pulsed ENDOR technique proposed by Mims (*1*) is based on the stimulated ESE sequence (see Fig. 1a). To understand qualitatively the origin of the ENDOR effect in this technique, we have to consider the precession of the electron spins in a coordinate frame (XYZ) rotating around axis Z // $\mathbf{B_o}$ with the frequency equal to the carrier frequency of the mw pulses. Axis X of this frame is parallel to the mw field $\mathbf{B_1}$ and axis Y is perpendicular to X and Z. For simplicity, we will consider all the mw pulses to have the rotation angles of 90° in a clockwise direction.

The first two mw pulses separated by the time interval τ create a distribution of the Z-magnetization (so-called population (or absorption) grating (*5, 7*)) proportional to $-\cos(2\pi\nu\tau)$, where ν is a spin offset from the resonance in frequency units. The third mw pulse applied in time T after the second one transfers this Z-magnetization pattern into the XY plane. The Y-magnetization, M_Y, associated with every spin isochromate then evolves in proportion with $-\cos(2\pi\nu\tau)\cdot\cos(2\pi\nu t)$, where t is a time interval after the third mw pulse. The latter expression can be written as

$$M_Y \propto -\cos[2\pi\nu(t-\tau)] - \cos[2\pi\nu(t+\tau)]. \qquad [5]$$

The macroscopic value of the Y-magnetization, $\langle M_Y\rangle$, is obtained by averaging Eq. [5] over ν. The second term in Eq. [5] describes an FID signal. For a distribution of ν broader than $1/\tau$ (the situation typical for ESE experiments with paramagnetic centers stabilized in solid matrices) its contribution to $\langle M_Y\rangle$ is negligible.

The first term in Eq. [5] is also about zero for any t significantly differing from τ. For t close to τ, however, it becomes essentially independent of ν and the averaging gives $\langle M_Y\rangle = -1$ implying a convergence of the electron spins along $-Y$ and a formation of the stimulated ESE signal with an amplitude V that attains its maximum at $t = \tau$.

Let us consider what happens if an RF pulse is introduced between the second and third mw pulses. The RF pulse is assumed to have a flip angle of 180° (which corresponds to a maximum ENDOR effect (*3*)) and to be in resonance with a transition of a magnetic nucleus ($I = \frac{1}{2}$) coupled to the ESE-forming electron spins with a hfi constant A. the RF-induced change of the nuclear spin projection leads to the change of the electron spin precession frequency from ν to $\nu' = \nu \pm A$. Now for the Y-magnetization after the third mw pulse we have to write

$$\begin{aligned} M_Y &\propto -\cos[2\pi\nu\tau]\cos[2\pi(\nu \pm A)t] \\ &\propto -\cos[2\pi\nu(t-\tau) \pm 2\pi At] \\ &\quad -\cos[2\pi\nu(t+\tau) \pm 2\pi At] \end{aligned} \qquad [6]$$

and the amplitude of the stimulated ESE signal at $t = \tau$ obtained by averaging Eq. [6] over ν is given by

$$V \propto \cos(2\pi A\tau). \qquad [7]$$

The change of the stimulated ESE signal amplitude described by Eq. [7] represents the ENDOR effect.

We have assumed above that each electron spin contributing to the ESE signal is coupled to a nuclear spin affected by the RF pulse. If the RF pulse inverts the nuclear spins coupled to only a

fraction $p \leq 1$ of the electron spins, the ESE signal will be contributed by the electron spins coupled to the nuclear spins inverted by the RF pulse (statistic weight p) and those coupled to the nuclear spins unaffected by the RF pulse (statistic weight $(1 - p)$). The sum of these two contributions gives

$$V \propto (1 - p) + p \cos(2\pi A\tau) = 1 - p[1 - \cos(2\pi A\tau)]. \quad [8]$$

A very important source of $p < 1$ is related to the fact that the whole electron spin ensemble may be described as a coherent superposition of the electron spins with the projections $m_S = \frac{1}{2}$ and $-\frac{1}{2}$. The transition frequencies of the nuclei coupled to these electron spin manifolds are different ($\nu_I - A/2$ and $\nu_I + A/2$ for a nucleus with $I = \frac{1}{2}$ coupled to the electron spins with $m_S = \frac{1}{2}$ and $-\frac{1}{2}$, respectively). In an experiment, usually only the nuclei with one of these frequencies are inverted by the RF pulse thus leading to a maximum value of $p = \frac{1}{2}$ even for narrow isotropic nuclear transitions. Further decrease of the p-value may arise for broad ENDOR lines, e.g., due to the anisotropy of a hyperfine interaction in solid matrices.

To separate the two sources of the incomplete nuclear spin inversion, we may split the factor p into two terms, p_+ and p_-, corresponding to the nuclei coupled after the second mw pulse to the electron spins with $m_S = \frac{1}{2}$ and $-\frac{1}{2}$, respectively. For a 180° RF pulse, the values $p_\pm \leq \frac{1}{2}$ are determined by the hfi anisotropy. The hfi constants corresponding to these nuclear spin populations will also be written separately as A_+ and A_-, even if they are usually the same and equal to A. The final expression for the stimulated ESE amplitude then becomes

$$V = 1/2[V^+ + V^-] \propto 1/2(1 - 2p_+[1 - \cos(2\pi A_+\tau)] + 1 - 2p_-[1 - \cos(2\pi A_-\tau)]), \quad [9]$$

where V^+ and V^- are the contributions of the electron spin subensembles that, after the second mw pulse, have the projections of $\frac{1}{2}$ and $-\frac{1}{2}$, respectively. These values will be referred to as the fractional ESE amplitudes. For well-separated ENDOR lines, like those arising due to α- or β-protons in aromatic organic radicals, one of the p-values, p_+ or p_-, equals zero and the values A_+ and A_- are equal if only one radiofrequency is used to invert the nuclear spins.

Equations [8], [9] reproduce a well-known result (*1, 3–8*) that the ENDOR spectrum amplitude is modulated with a period $1/\tau$, giving a maximum effect at the hfi values $A = \pm[\frac{1}{2} + n]/\tau$ (where $n \geq 0$ is an integer number) and blind spots at $A = \pm n/\tau$. An undistorted spectrum can be obtained as a sum of the spectra recorded at several τ values. Another obvious technique is to make τ as short as possible, so that the first blind spot is outside the spectrum range of interest. In this case, if τ is shorter than the spectrometer dead time, t_d, one may introduce a fourth (180°) mw pulse in time $t' > t_d$ after the stimulated ESE signal in order to refocus it and make it observable. To our knowledge, this technique was first used in (*14*). Later it was described in detail in (*15*), where it was called refocused Mims (ReMims) ENDOR. However, as follows from Eqs. [8], [9], the ENDOR effect becomes small for short τ values, which represents a disadvantage of this technique.

As one can see from Eqs. [8], [9], the ENDOR effect in a spectrum recorded at any τ value should tend to zero for small hfi constants A. However, very often a most prominent feature in the experimental Mims ENDOR spectra of paramagnetic centers stabilized in matrices containing many hydrogen nuclei is a peak at the Zeeman frequency of protons (see, e.g., Fig. 3a). As mentioned in the Introduction, no satisfactory explanation of this seeming discrepancy between the theory and an experiment has been given in the literature.

Before considering the origin of the matrix line, we have to mention some general properties of the Mims ENDOR spectrum. If several nuclei contribute to the same region of the ENDOR spectrum but they are coupled to different electron spins, a simultaneous inversion of these nuclear spins results in an increase of the p-values in Eqs. [8], [9] as given by $p = \Sigma_j p_j$. The ENDOR effect in this case is additive with respect to the nuclear contributions.

On the other hand, if several nuclei interact with the same electron, the change of the local magnetic field for the electron is additive with respect to the contributions of separate nuclei, $A = \Sigma_j c_j A_j$, where the factors c_j are equal to 1 or -1, depending on the sign of the change of the spin projection of the jth nucleus in an RF-induced transition. There will be no increase in the p-values in this case and the ENDOR effect will not change in amplitude, but its dependence on τ will show a distribution of the oscillation frequencies corresponding to the distribution of c_j values. At a high temperature ($h\nu_I \ll kT$, where T is temperature and k is a Boltzmann constant) the latter distribution is binomial and the fractional ESE amplitudes are obviously expressed in a compact way as $V^\pm = \Pi_j V_j^\pm$ as it is also obtained from the density matrix considerations (*3*).

We also have to discuss an important difference between the distant matrix nuclei and the nuclei situated in a close vicinity of the unpaired electron. In the latter case, the number of nuclei is relatively small and they are usually arranged in a regular manner with respect to the molecular coordinate frame. If the hyperfine interactions of these nuclei are anisotropic, the total spectra of their transitions at different orientations of the molecular frame will generally be different. Thus, by applying an RF irradiation in resonance with any particular region in the spectrum of the nuclear transitions, we will change the local magnetic fields for only a fraction ($p < 1$ in Eq. [8] or $p_+ < \frac{1}{2}$, $p_- < \frac{1}{2}$ in Eq. [9]) of the electrons contributing to the ESE signal.

The spatial arrangement of the distant matrix nuclei, on the other hand, is approximately uniform and isotropic and the nuclear transition spectrum does not depend on the orientation of the molecular frame. The RF irradiation applied to any part of the spectrum of these nuclei will change the local field for

all the unpaired electrons. By definition, this means $p = 1$ in Eq. [8] and $p_+ = p_- = \frac{1}{2}$ in Eq. [9]. Thus, for the distant matrix nuclei it is appropriate to write

$$V = 1/2[V^+ + V^-] \propto 1/2[\cos(2\pi A_+\tau) + \cos(2\pi A_-\tau)]. \quad [10]$$

3. Matrix Line in Mims ENDOR

To explain the "anomalous" intensity of the matrix line we have to take into account a large number of distant matrix nuclei. A 180° RF pulse inverts the orientations of all the resonant nuclei. The effect of this inversion on the local magnetic field and precession frequency of the unpaired electron is additive, $\Delta\nu = \Delta M_I D$, where ΔM_I is a change of the total nuclear spin projection. The average numbers of matrix nuclei coupled with an anisotropic hfi constant D to the unpaired electrons with $m_S = \frac{1}{2}$ and $-\frac{1}{2}$ will be denoted by N_+ and N_-, respectively. These nuclei may have different spin projections m_I. We will call a given realization of the nuclear spin projections in an ensemble of $N_\pm$ nuclei a nuclear spin configuration. The total spin projection M_I for a given nuclear spin configuration is a sum of the spin projections of individual nuclei.

In a high temperature approximation ($h\nu_I \ll kT$) all nuclear spin configurations are realized with equal probabilities. This leads to the binomial distribution of M_I with a probability $P_\pm(M_I)$,

$$P_\pm(M_I) = (1/2^{N\pm})N_\pm!/n!(N_\pm - n)!, \quad [11]$$

where $0 \le n \le N_\pm$ is the number of nuclei with $m_I = \frac{1}{2}$. For large $N_\pm$ this distribution tends to the Gaussian one:

$$P^\pm(M_I) = (2/\pi N_\pm)^{1/2}\exp[-2(n - N_\pm/2)^2/N_\pm]. \quad [12]$$

The total nuclear spin projection enters Eqs. [11], [12] implicitly as $M_I = n - N_\pm/2$. The change of M_I, $\Delta M_I = 2M_I = 2n - N_\pm$, is thus weighted with the factor $P_\pm(M_I)$ and the ESE signal is calculated as a sum over various nuclear spin configurations,

$$V = 1/2[V^+ + V^-] \propto 1/2\,[\textstyle\sum_n P_+(M_I)\cos[2\pi(2n - N_+)D\tau] + \sum_n P_-(M_I)\cos[2\pi(2n - N_-)D\tau]]. \quad [13]$$

The oscillating terms in Eq. [13] represent the expansions of $P_\pm(M_I)$ into a cosine Fourier series. Using Eq. [12], one can find that for large enough $N_\pm$ the dependence of the stimulated ESE signal on τ will be described by a sum of Gaussian functions:

$$V = 1/2[V^+ + V^-] \propto 1/2[\exp(-2\pi^2 N_+ D^2\tau^2) + \exp(-2\pi^2 N_- D^2\tau^2)]. \quad [14]$$

With increasing τ, the ESE amplitude tends to zero. This explains the appearance of an intense matrix line in the Mims ENDOR spectra.

Let us estimate the number of nuclei $N_\pm$ that have dipole interactions in the range from $D - \Delta D$ to $D + \Delta D$ ($\Delta D \ll D$). The non-zero width of the RF excitation, $2\Delta D$, is contributed by two factors. The less significant one is a homogeneous broadening of the proton transitions that might be of the order of several kilohertz. The second (and, usually, much more significant) factor is related to the finite RF pulse width. We will assume for certainty that the carrier frequency of the RF pulse, ν_{rf}, is greater than ν_I. This means that in order to be in resonance with the RF pulse, the nuclei coupled to the $m_S = \frac{1}{2}$ and $-\frac{1}{2}$ electron spin manifolds should have negative and positive signs of the dipole interaction, respectively.

For any given distance R from the unpaired electron, the nuclei are in resonance with the RF pulse if they are located at the angles θ satisfying the condition

$$D_o[1-3\cos^2\theta] = D_{res}, \quad [15]$$

where $D_{res} \in [D - \Delta D, D + \Delta D]$. Using Eq. [15], it is easy to find a maximum value of the distance, R_{max}, at which the nuclei still can be in resonance. Substituting $\theta = 0°$ (or $\theta = 180°$) into Eq. [15] we can find for the nuclei coupled to the $m_S = -\frac{1}{2}$ electron spin manifold

$$R_{max} = |2g_e g_N\beta_e\beta_N/hD_{res}|^{1/3}. \quad [16]$$

For the nuclei coupled to $m_S = \frac{1}{2}$, after substituting $\theta = 90°$ into Eq. [15], we find

$$R_{max} = |g_e g_N\beta_e\beta_N/hD_{res}|^{1/3}. \quad [17]$$

The number of resonant nuclei is then calculated as

$$N_\pm = 4\pi\rho\left[\int_0^{R_{out}} R^2 dR \int_{\theta_{min}}^{\theta_{max}} \sin\theta d\theta - \int_0^{R_{inn}} R^2 dR \int_{\theta_{min}}^{\theta_{max}} \sin\theta d\theta\right], \quad [18]$$

where ρ is a density of nuclei in a sample. R_{out} and R_{inn} are the R_{max} values for $D_{res} = D - \Delta D$ and $D_{res} = D + \Delta D$, respectively. The angles θ_{min} for N_- and θ_{max} for N_+ are equal to 0° and 90°, respectively. The angles θ_{max} for N_- and θ_{min} for N_+ are expressed in terms of R using Eq. [15]. The factor of 4π, instead of 2π, in front of the integrals takes into account the fact that the angles θ in Eq. [18] do not exceed 90°. The integration gives

$$N_+ = N_- = [16/243^{1/2}]\pi\rho g_e g_N\beta_e\beta_N\Delta D/[h(D^2 - \Delta D^2)]. \quad [19]$$

As ΔD is assumed to be much less than D and the numerical factor in the expression for $N_{\pm}$ is close to unity (about 1.03), Eq. [19] may be reduced to

$$N_{\pm} \approx \pi\rho g_e g_N \beta_e \beta_N \Delta D/hD^2 \qquad [20]$$

which finally results in

$$V \propto \exp(-2\pi^3\rho g_e g_N \beta_e \beta_N \Delta D\tau^2/h) = \exp(-\tau^2/2\tau_{dec}^2), \quad [21]$$

where

$$\tau_{dec} = [h/(4\pi^3\rho g_e g_N \beta_e \beta_N \Delta D)]^{1/2}. \qquad [22]$$

One can see that, as long as $D \gg \Delta D$, the power of the exponent in Eq. [21] does not depend on D and is linear with respect to ΔD. If we split ΔD into a sequence of smaller intervals δD_k, so that $\Delta D = \Sigma_k \delta D_k$, we will see that $V^{\pm} = \Pi_k V_k^{\pm}$ and the distribution of the dipole interactions associated with the region ΔD is a convolution of the distributions associated with δD_k. This is a natural consequence of the statistical independence of nuclear subensembles corresponding to different δD.

For small values of D our approach based on the assumption of $D \gg \Delta D$ and, correspondingly, a very small relative variation of the dipole interaction within the range of the RF excitation becomes inapplicable. In particular, it is not applicable directly to the case of $\nu_{rf} = \nu_I$ ($D = 0$). To include this situation into our analysis, we have to note that in practice the width of the matrix line $\Delta\nu_m$ is always finite and the ΔD value may always be chosen much smaller than $\Delta\nu_m$. We can show that under these conditions the ESE dependence on τ for the case of $D = 0$ is also expressed by Eq. [21]. For this, we can split the excited region of the dipole interactions from 0 to ΔD (for the region from $-\Delta D$ to 0 similar considerations apply) into an infinite sequence of regions with the widths of $2\delta D_k$ and central D-values of D_k, so that $\Delta D = 2\Sigma_k \delta D_k$ and $\delta D_k/D_k = r \ll 1$, where r is a positive constant. The values D_k are expressed as

$$D_k = \Delta D(1 - r)^{k-1}/(1 + r)^k \qquad [23]$$

and tend to zero with increasing k. At this point our discussion is still purely theoretical and we have a freedom in the choice of ΔD. From Eqs. [19], [20] it follows that for any $r \ll 1$ we can always select ΔD to be small enough to ensure that the number of nuclei contributing into the outmost interval δD_1 is sufficiently large to provide for the validity of the Gaussian approximation. The number of nuclei contributing into the interval δD_k becomes greater with increasing k (see Eqs. [19], [20]), so that the Gaussian approximation (Eq. [12]) remains valid for every k, as well as Eq. [21], where we have to write δD_k on place of ΔD. Taking products of the ESE decays as given by $V^{\pm} = \Pi_k V_k^{\pm}$ (where the $V_k^{\pm}$ are the Gaussian functions) is equivalent to the summation of the infinite geometric progressions of $\delta D_k = rD_k$ for the intervals from $\pm\Delta D$ to 0 in the power of the exponent, and finally results in Eq. [21]. The above considerations prove that, at least for small enough ΔD values (as compared with the matrix linewidth), the dependence of the stimulated ESE signal on τ is described by a Gaussian function given by Eq. [21]. The question as to what ΔD may be considered small enough for any practical situation (including the choice of the nuclear density ρ) is, however, to be answered by means of numerical calculations that will be discussed below.

By substituting $A = (2n - N_{\pm})D$ into Eq. [12] and renormalizing it to a unity integral or by Fourier-transforming Eq. [21] we can find the distribution of the local fields A associated with the nuclear spins inverted by the selective RF pulse:

$$P(A) = (2/\pi A_o^2)^{1/2}\exp[-2A^2/A_o^2]. \qquad [24]$$

The width A_o of this distribution equals

$$A_o = 2(\pi\rho g_e g_N \beta_e \beta_N \Delta D/h)^{1/2}. \qquad [25]$$

The above analysis explains the matrix ENDOR effect and its dependence on parameters related to the experimental conditions (ΔD, τ) and sample properties (ρ). There are, however, several limitations and corrections that have to be mentioned.

The matrix nuclei (e.g., protons) are distributed around the unpaired electron starting from some minimal distance R_{min} that in many cases may be estimated as $R_{min} \approx 2 \div 4$ Å (see (*16*) and references therein). For weak dipole interactions, the assumption of $R_{min} = 0$ made above does not change significantly the estimate of $N_{\pm}$. However, at the D-values close to those corresponding to R_{min}, the number of nuclei becomes small thus making the Gaussian distribution (Eq. [12]) used in the analysis inapplicable. The averaging of the electron spin precession frequencies in Eq. [13] in this case becomes incomplete and, instead of the Gaussian damping of the ESE intensity, oscillations might appear.

As a result of the failure of the Gaussian approximation for short distances, our analysis cannot be extrapolated to the case of a non-selective RF excitation of all the matrix nuclei. It is well known that in the latter case the local field distribution is close to Lorentzian (*17*) and, consequently, the ESE decay is close to exponential, as demonstrated by pulsed electron–electron double resonance (ELDOR) (*18*) and "2 + 1" ESE (*19*) experiments that are ideologically similar to the Mims ENDOR (in the ESE ELDOR and "2 + 1" experiments two electron subensembles are considered, one of which plays the same role as the nuclear ensemble in ENDOR). However, we will show below by means of direct numerical simulations that

both types of ESE decays, Gaussian and exponential, can be realized depending on the RF excitation range.

In our treatment we have assumed a uniform inversion of the nuclear spins by the RF pulse within a frequency region corresponding to the range of the dipole coupling values of $2\Delta D$. In reality, however, the nuclear spin inversion is not uniform. Using a density matrix formalism, one can easily derive that after an RF pulse of the duration t_{rf} the nuclear spin projection on $\mathbf{B_o}$ is described by the expression

$$M_Z(\Delta\nu) = 1 - 2(\nu_2^2/\nu_N^2)\sin^2(\pi\nu_N t_{rf}), \qquad [26]$$

where $\Delta\nu$ is an offset of the nuclear spin from resonance, $\nu_2 = g_N\beta_N B_2/h$ is an RF field intensity, and $\nu_N = (\nu_2^2 + \Delta\nu^2)^{1/2}$ is a nutation frequency of the nuclear spins during the RF pulse. The second term in this expression (without the numerical factor of 2) represents a probability to invert a nuclear spin at a given offset from the resonance. In effect, this term decreases the density of nuclear spins at large offsets from the resonance. Taking into account the realistic excitation profile of the RF pulse analytically represents a formidable problem. However, Eq. [26] is readily incorporated into the numerical simulations that will be discussed in the next section.

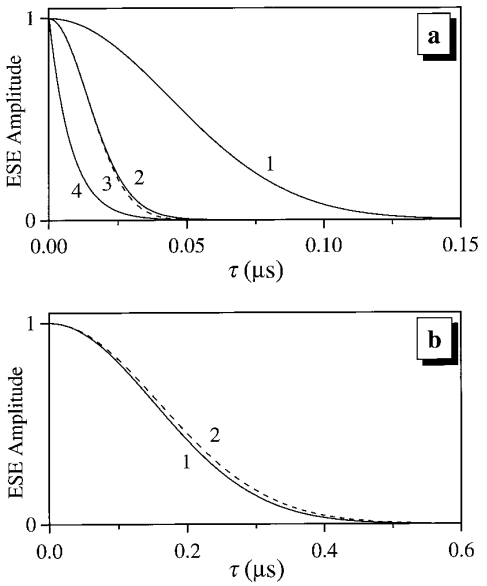

FIG. 2. (a) The dependences of the stimulated ESE amplitude on τ calculated as explained in the text for a uniform RF excitation with $D = 0$ MHz and $\Delta D = 1$ MHz (trace 1), 10 MHz (trace 2), and 1000 MHz (trace 4). Dashed trace 3 is calculated using Eq. [21]. (b) The dependences of the stimulated ESE amplitude on τ calculated as explained in the text for an RF excitation profile described by Eq. [26] with $\nu_2 = 0.039$ MHz and $t_{rf} = 10$ μs (trace 1) and 12.8 μs (trace 2). The center of the RF resonance was at $D = 0$ MHz and the dipole interaction range taken into account was $\Delta D = 1$ MHz.

4. Numerical Calculations of the Matrix Mims ENDOR Effect

The purpose of the numerical simulations that we perform in this section is to calculate the dependences of the matrix Mims ENDOR effect on τ for various values of the RF excitation range ΔD and to see how far the limits of the applicability of Eq. [21] really extend. Another purpose of the calculations is to elucidate the effect of the realistic RF excitation profile given by Eq. [26].

In the calculations we will assume the RF pulse to be exactly in resonance with the nuclear Zeeman frequency ($D = 0$). The nuclear ensemble will consist of protons uniformly distributed with a density ρ of 0.05 Å^{-3}, which represents a fair order-of-magnitude approximation for many organic and inorganic substances. The strategy of the calculation is, the same as in our theoretical treatment above, to split ΔD into a series of smaller intervals $D_k \pm \delta D_k$ (see Eq. [23]), find for them $N_{k\pm}$ using Eq. [19], and calculate the ESE signal as $V^{\pm} = \Pi_k V_k^{\pm}$, where the $V_k^{\pm}$ are the ESE signals for every δD_k described by Eq. [13].

There is a difficulty in this approach related to the fact that the estimated number of nuclei $N_{k\pm}$ may be non-integer and, for large D_k and/or very small δD_k values, it may even be less than unity. The binomial distributions (Eq. [12]) expressed through the factorials of integer numbers then become inapplicable. Though one can possibly overcome this difficulty by substituting the factorials by Γ-functions, we have chosen a different approach which appears to be more physical and more easily justifiable. We postulate that $N_{k\pm}$ found using Eq. [19] is, actually, an *average* (over various realizations of nuclear arrangements around all the unpaired electrons in the system) number of nuclei with a dipole interaction in the interval $D_k \pm \delta D_k$. For given $N_{k\pm}$, the probability $p(m, N_{k\pm})$ to find m nuclei satisfying the same condition for the dipole interaction in vicinity of the unpaired electron may then be estimated as given by Eq. [A3] (see Appendix).

Thus, at the kth step of the calculation, we estimate $N_{k\pm}$ from the values of D_k (see Eq. [23]) and $\delta D_k = rD_k$, where $r \ll 1$ is a positive constant (a typical value of r used in the calculation was 0.025, though the final result of the calculation did not depend on r). The ESE signals for various m are calculated using Eqs. [11]–[13] with $N_{\pm}$ being substituted by m, and D substituted by D_k. Then these signals are summed (because different m correspond to different electrons) with statistic weights $p(m, N_{k\pm})$ to obtain the total dependences $V_k^{\pm}(\tau)$ for the given dipole interaction interval. The index k in the calculation is incremented until D_k becomes smaller than 10^{-6} MHz. The product of $V_k^{\pm}(\tau)$ for all intervals finally results in the observable τ-dependence of the matrix Mims ENDOR effect.

The results of the calculations for several ΔD values are shown in Fig. 2a. Trace 1 gives a τ-dependence for $\Delta D = 1$ MHz. A numerical function fitting shows that this dependence is almost perfectly Gaussian with τ_{dec} described by Eq. [22], the same as those calculated for smaller ΔD values (not shown). Trace 2 shows a τ-dependence for $\Delta D = 10$ MHz calculated as described above and dashed trace 3 is calculated

using Eq. [21] with a direct substitution of $\Delta D = 10$ MHz. One can see that even for $\Delta D = 10$ MHz the τ-dependence is very closely Gaussian with τ_{dec} close to that determined by Eq. [22]. A further increase in ΔD-values leads to taking into account a very small number of close nuclei in the calculation and to the gradual transition of the dependence to the exponential one (see trace 4 calculated for $\Delta D = 1000$ MHz), as expected from the general considerations (see the discussion above and Refs. (*17–19*)). A direct exponential fitting shows that the characteristic decay time of the exponent is about 0.008 μs in agreement with that predicted theoretically for the case of a non-selective RF pulse (*18, 19*):

$$\tau_{dec} = 243^{1/2}h/(16\pi^3\rho g_e g_N \beta_e \beta_N). \qquad [27]$$

It is interesting to note that if we take $\Delta D = 10$ MHz and select $D_1 = 8$ MHz and $\delta D_1 = 2$ MHz at the first calculation step, we can estimate the number of nuclei $N_{1\pm} \approx 0.4$ (for $\rho = 0.05$ Å^{-3} used in our calculation). We can see that, while the validity of the condition $\delta D_1 \ll D_1$ is already questionable, the condition $N_{1\pm} \gg 1$ is violated completely. For this particular case it is obviously impossible to choose δD_1 and D_1 in such a way that the conditions $\delta D_1 \ll D_1$ and $N_{1\pm} \gg 1$ were satisfied simultaneously. Still, the comparison of traces 2 and 3 in Fig. 2a shows that the τ-dependence of the ESE signal is nearly Gaussian indicating that the adverse effects of close nuclei are only minor even for this large ΔD value.

It follows from our calculations (not shown) that a decrease in the nuclear density ρ leads to a decrease of the ΔD values for which the Gaussian ESE decay will still be observed. For example, for a very practical choice of $\Delta D = 0.1$ MHz the ESE decay becomes noticeably non-Gaussian for $\rho \leq 10^{-4}$ Å^{-3}. This proton density is two orders of magnitude lower than that normally encountered in experiments. Therefore, we expect that for the majority of practical situations a Gaussian ESE decay will be observed in experiments.

Another important problem we will discuss is the influence of the RF excitation profile on the ESE decays. Setting up a pulsed ENDOR experiment usually requires the adjustment of the RF pulse duration (t_{rf}) for a given RF amplitude (ν_2) in order to achieve a maximum ENDOR effect. Integrating Eq. [26] over $\Delta\nu$ from $-\infty$ to $+\infty$ (which is justified by the fact that the matrix line is usually much broader than the main lobe of the RF excitation spectrum) allows one to find that the maximum average spin inversion is achieved at the nominal flip angle $\theta_{rf} \approx 140°$. However, it is not clear in advance if the RF pulse with t_{rf} corresponding to $\theta_{rf} \approx 140°$ will also lead to a fastest Gaussian decay and to a maximum ENDOR effect for any given τ value. Clarifying this problem also represents a purpose of the calculations below.

In the calculations we have taken $t_{rf} = 10$ μs and $\nu_2 = 0.039$ MHz to provide $\theta_{rf} \approx 140°$. We found that for the matrix linewidth $\Delta\nu_m \geq 0.5$ MHz (corresponds to the minimum electron-nuclear distance $R_{min} \leq 5.4$ Å), the calculation result practically did not depend on $\Delta\nu_m$. The main change of τ_{dec} (only about 2%) was observed upon increase of $\Delta\nu_m$ from 0.5 to 1 MHz. The ESE decay calculated for $\Delta\nu_m = 1$ MHz is shown by trace 1 in Fig. 2b. Trace 2 in Fig. 2b was calculated for $t_{rf} = 12.8$ μs ($\theta_{rf} \approx 180°$) to demonstrate that, indeed, the ENDOR effect for the matrix line attains its maximum for $\theta_{rf} \approx 140°$ even taking into account its dependence on τ.

In order to be able to qualitatively analyze the experimental data on matrix ENDOR without performing each time this type of numerical calculations, we will introduce an effective width of a uniform RF excitation in the form $\Delta D = \alpha/t_{rf}$, where α is a phenomenological parameter. A criterion to choose α is a coincidence of the ESE decay obtained in the calculation for a real excitation profile with that obtained in the calculation for a uniform excitation profile. Our calculations show that for an RF pulse with $\theta_{rf} \approx 140°$ an equivalent uniform excitation width is $\Delta D \approx 0.86/t_{rf}$ ($\alpha \approx 0.86$). Taking into account this result, we may write for the characteristic time of the Gaussian decay obtained with an RF pulse of the duration t_{rf}

$$\tau_{dec} \approx [ht_{rf}/(3.4\pi^3\rho g_e g_N \beta_e \beta_N)]^{1/2}. \qquad [28]$$

In the next section we will use this expression to estimate the proton density from the experimental ESE decay.

5. *Experimental Measurements of the Matrix Mims ENDOR Effect*

For the experimental verification of the theoretical results obtained above we have measured the dependence of the matrix Mims ENDOR effect on τ and t_{rf}. As an object for the measurements we have used the radicals $C^{\bullet}H(COOH)_2$ and $C^{\bullet}H_2COOH$ stabilized in a γ-irradiated malonic acid powder. These radicals give overlapping EPR spectra with a dominating doublet feature due to the hfi of the α-proton in the $C^{\bullet}H(COOH)_2$ radical (*20, 21*). Figure 3a shows a Mims ENDOR spectrum obtained as follows. First, the dependences of the stimulated ESE signal on τ were recorded under the RF irradiation with various ν_{rf} (t_{rf} and ν_2 were adjusted to provide a maximum ENDOR effect). Then these traces were normalized by the dependence of the stimulated ESE signal on τ without RF irradiation. The ENDOR traces at τ values from 128 to 2320 ns have been summed up to give the spectrum shown in Fig. 3a. The most prominent feature in this spectrum is the line due to the distant matrix protons situated in a frequency range from about 14.6 to 15 MHz, symmetrically with respect to the proton Zeeman frequency (about 14.8 MHz in the applied magnetic field of 348 mT).

Traces A, B, and C in Fig. 3b show the dependences of the ESE signal on τ corresponding to ν_{rf} of 15.6, 14.5, and 14.8 MHz, respectively. These frequency positions are marked in Fig. 3a by arrows labelled with the same capital letters. One can see a striking difference between these traces. Trace A

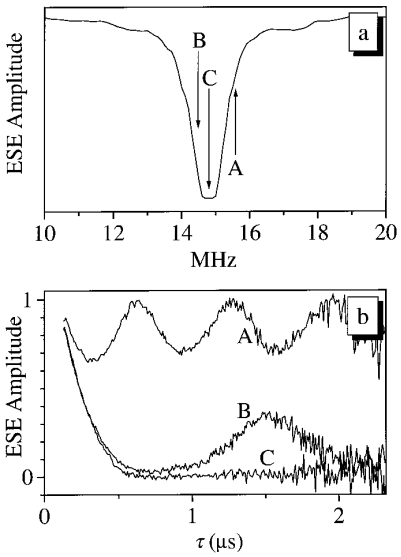

FIG. 3. (a) The Mims ENDOR spectrum of the radicals in a γ-irradiated malonic acid powder (see text for detailed explanations). Arrows labeled A, B, and C correspond to the frequencies of 15.6, 14.5, and 14.8 MHz, respectively. (b) Traces A, B, and C, the dependences of the stimulated ESE amplitude on τ obtained under the RF pumping at the frequencies of 15.6, 14.5, and 14.8 MHz, respectively. The dependences have been normalized by the ESE decay obtained without the RF irradiation.

corresponds to relatively strongly coupled protons and shows an oscillation with a frequency of about 1.6 MHz, as predicted by Eq. [8]. On the other hand, trace C corresponds to distant matrix protons and exhibits a fast monotonous decrease of the ESE signal intensity.

According to Eq. [21], the ESE signal intensity measured under the RF irradiation of the matrix proton region (and normalized by the relaxation decay) should show a Gaussian decay with increasing τ. To check this, we have performed the measurements of the ESE decay for several RF pulse durations (adjusted to give a maximum ENDOR effect at selected RF power levels). Figure 4a shows the normalized experimental ESE decays (noisy traces) and Gaussian fits to them (smooth lines). The traces with faster decays in Fig. 4a correspond to shorter RF pulses. One can see from comparison that, indeed, in agreement with Eq. [21], a Gaussian function represents a very good approximation to the experimental ESE decays obtained under the RF pumping of the matrix proton line.

From Eq. [28], τ_{dec} is expected to be proportional to the square root of t_{rf}. Filled circles in Fig. 4b show the correspondence between the values of τ_{dec} obtained from the Gaussian fitting of the experimental ESE decays in Fig. 4a and the square roots of t_{rf} values used in the experiment. The linear relation obtained supports the validity of our analysis.

Finally, it is interesting to estimate the average density ρ of the matrix protons from the experimental data shown in Fig. 4b. Substituting into Eq. [28] the value of $g_e g_N \beta_e \beta_N / h \approx 79$ MHz · Å^3 corresponding to protons, the experimental values of t_{rf} and τ_{dec} shown in Fig. 4b, one can find $\rho \approx 0.031$ Å^{-3}. This value is in a reasonable agreement with the estimate of the proton density in a malonic acid powder, $\rho \approx 0.037$ Å^{-3}, obtained from the molecular structure of malonic acid and its specific weight of 1.619 g/cm^3 (*22*).

Substituting $\Delta D \approx 0.06$ MHz (for $t_{rf} = 13$ μs used to record the ENDOR spectrum in Fig. 3a) into Eq. [20] we can estimate the number of nuclei $N_{\pm}$ contributing into the matrix line at $D = 0.6$ MHz to be about 1.5 and $N_{\pm} \approx 6$ at $D \approx 0.3$ MHz. This sets the limits of the applicability of the Gaussian approximation in our analysis to the D-values not exceeding 0.3 MHz for the given ρ and t_{rf}. An example of the incomplete averaging of the electron spin precession frequencies in Eq. [13] due to a too small number of simultaneously inverted nuclei is shown by trace B in Fig. 3b corresponding to $D = 0.6$ MHz and exhibiting a damped irregular oscillation in agreement with the above general considerations.

6. *Matrix Line in Davies ENDOR*

Let us consider briefly the matrix line in Davies ENDOR. The pulse sequence usually employed is shown in Fig. 1b. Same as the Mims ENDOR sequence (Fig. 1a), it consists of three mw pulses. Now, however, these pulses are selective and their functions are different from those in Mims ENDOR. The first (180°) pulse inverts the electron spins in a close vicinity of the exact resonance. One often says in this case that this pulse burns a hole in the EPR spectrum.

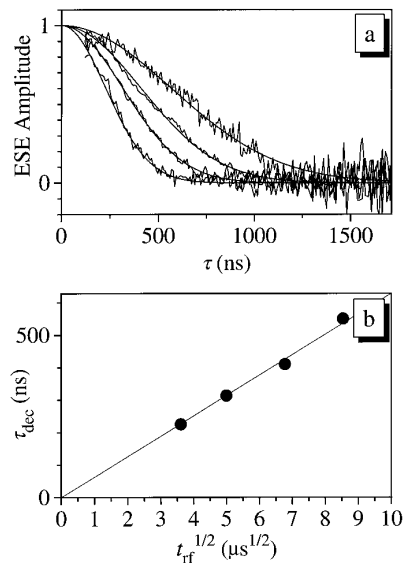

FIG. 4. (a) Noisy traces, the dependences of the stimulated ESE amplitude on τ obtained under the RF pumping at the frequency of 14.8 MHz. The RF pulse widths are 13, 25, 46, and 73 μs, with the shorter RF pulses corresponding to the faster decays. The dependences have been normalized by the ESE decay obtained without the RF irradiation. Smooth lines, Gaussian fits to the experimental traces with the characteristic decay times τ_{dec} of 225, 313, 410, and 550 ns. (b) Filled circles, the dependence of τ_{dec} on the square root of the RF pulse duration. Solid line, linear least squares fit to the experimental points.

When a 180° RF pulse is applied after the first mw pulse, it exchanges the populations between the electron-nuclear sublevels in resonance with the RF pulse. As a result, the original hole decreases in amplitude and a pair of new holes appears at the spectrum positions $\pm A$ with respect to the original (central) hole (for a detailed discussion see, e.g., (*6*)). The amplitudes of the resulting holes depend on the fraction of the electron spins coupled to the nuclei inverted by the RF pulse, i.e., on the p-values introduced above. If we assume the amplitude of the EPR spectrum before the first mw pulse to be $E(\Delta\nu_e) = 1$ ($\Delta\nu_e = g_e\beta_e\Delta B_o/h$ is an offset of the electron spin from resonance) and after the inversion $E(0) = -1$, then after the RF pulse the amplitudes of the EPR spectrum in the holes will be

$$E(0) = -1 + 2p; \qquad E(\pm A) = 1 - p. \qquad [29]$$

The shape of the original hole produced by a rectangular mw pulse is described by the expression similar to Eq. [26],

$$E(\Delta\nu_e) = 1 - 2(\nu_1^2/\nu_N^2)\sin^2(\pi\nu_N t_p), \qquad [30]$$

where $\nu_1 = g_e\beta_e B_1/h$ is a mw field intensity, $\nu_N = (\nu_1^2 + \Delta\nu_e^2)^{1/2}$ is a nutation frequency of the electron spins during the mw pulse, and t_p is a duration of this pulse. For the first mw pulse with a nominal flip angle of 180°, the hole shape (more exactly, the central lobe) can be approximated by a Gaussian function:

$$E(\Delta\nu_e) \approx 1 - 2\exp(-\Delta\nu_e^2/\nu_1^2). \qquad [31]$$

We employ here a Gaussian approximation instead of a rational one used elsewhere (*7*) because it is more convenient from the mathematical viewpoint for estimation of the matrix ENDOR effect (see below).

After the RF pulse, the shapes of all the holes produced are described by similar functions and the whole spectrum may be written as

$$\begin{aligned} E(\Delta\nu_e) \approx 1 &- 2(1-p)\exp[-\Delta\nu_e^2/\nu_1^2] \\ &- p\exp[-(\Delta\nu_e - A)^2/\nu_1^2] \\ &- p\exp[-(\Delta\nu_e + A)^2/\nu_1^2]. \end{aligned} \qquad [32]$$

To a first approximation we may consider the ESE signal V generated by the selective detection sequence shown in Fig. 1b to be proportional to the amplitude of the EPR spectrum Eq. [32] at $\Delta\nu_e = 0$:

$$V \approx -1 + 2p(1 - \exp[-A^2/\nu_1^2]). \qquad [33]$$

For $A \ll \nu_1$ the ESE signal is close to -1 and the ENDOR effect defined as a difference of the ESE signal with and without RF irradiation is close to zero as noted in many publications on Davies ENDOR (*5–8*). Our purpose is to show that even in this case the ENDOR effect due to the distant matrix nuclei is non-zero. Its origin is exactly the same as that already discussed. That is, in the matrix region many nuclei are resonant with the RF pulse and the change of the local magnetic field associated with their simultaneous inversion is essentially non-zero.

As follows from our analysis of Mims ENDOR, to describe the effect due to the distant matrix nuclei, we have to take $p = 1$. The EPR hole shape in Eq. [32] at $p = 1$ represents a convolution of the original hole shape and a doublet spectrum with a splitting of $2A$. For the distant matrix nuclei inverted by an RF pulse, the distribution of A is described by Eq. [24]. Taking a convolution of the original EPR hole (Eq. [31]) with the Gaussian hfi distribution (Eq. [24]) we obtain

$$\begin{aligned} &E(\Delta\nu_e) \\ &\quad \approx 1 - 2\exp[-2\Delta\nu_e^2/(A_o^2 + 2\nu_1^2)]/[1 + A_o^2/(2\nu_1^2)]^{1/2}. \end{aligned} \qquad [34]$$

The amplitude of the ESE signal formed by a selective detection sequence is then approximately equal to

$$V = 1 - 2/[1 + A_o^2/(2\nu_1^2)]^{1/2}. \qquad [35]$$

We may estimate a realistic value of V for protons by taking $\rho \approx 0.05$ Å^{-3} (somewhat smaller than in water and greater than in the malonic acid), $g_e g_N \beta_e \beta_N/h \approx 79$ MHz · Å^3, $\Delta D \approx 0.1$ MHz (for an RF pulse with $t_{rf} = 8.6$ μs and $\theta_{rf} = 140°$) and $\nu_1 \approx 5$ MHz (for a 180° mw pulse of 100 ns duration). The width of the local field distribution A_o in this case is about 2.2 MHz and the value of V is about -0.8. Thus, the difference between the ESE signal amplitude with and without the RF irradiation makes up about 20% and is easily measurable.

This result may be compared with the ENDOR effect in a disordered solid matrix for the nucleus with $D_o = 2$ MHz and a_{iso} large enough to ensure that the side holes do not overlap with the central hole. The orientation of the radius-vector from the unpaired electron to the nuclear spin inverted by the RF pulse is taken close to perpendicular with respect to $\mathbf{B_o}$. For $\Delta D \approx 0.1$ MHz we can easily estimate the ESE amplitude V after the RF pulse to be about -0.88 implying an ENDOR effect of 12%, smaller than that obtained for the matrix line. In this calculation we have recalled that $p = p_+ + p_-$ (see above) and have taken p_+ (or p_-) equal to zero, which corresponds to the use of a single radiofrequency in an experiment.

7. Experimental Measurement of the Matrix Davies ENDOR Effect

The EPR hole broadening associated with the RF-induced inversion of the distant nuclear spins (or any other sources)

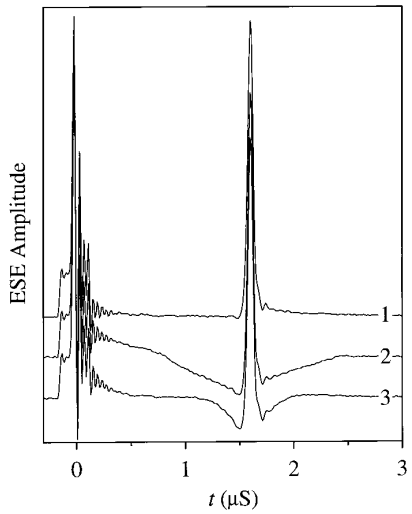

FIG. 5. The ESE signals formed by a detection sequence of two mw pulses with the durations of 16 and 24 ns in a sample of γ-irradiated malonic acid powder. Trace 1, no preparation mw pulse and no RF pulse are applied. Trace 2, a preparation mw pulse of 800 ns duration (180°) is applied 40 μs before the detection sequence. Trace 3, same as trace 2, but with an RF pulse of 9 μs duration (θ_{rf} = 140°) applied between the preparation mw pulse and the detection sequence.

can be directly observed using a nonselective detection pulse sequence (*23, 24*). The ESE signal formed by this sequence may be considered to consist of two contributions, a narrow intense signal with a positive amplitude due to the electron spins unaffected by the selective preparation pulse and a weak broad negative signal due to the EPR spectrum hole. The latter signal represents a Fourier image of the hole shape to a good accuracy. The RF-induced inversion of the matrix nuclear spins should lead to a broadening of the EPR spectrum hole described by Eq. [34], which can be detected as a narrowing of the negative component in the ESE signal.

To check the above considerations, we have done the Davies ENDOR experiment with a non-selective detection sequence using the γ-irradiated malonic acid powder as a sample. The mw sequence parameters have already been described in the Experimental section. Trace 1 in Fig. 5 shows the ESE signal in the absence of the preparation pulse. Trace 2 gives the ESE shape after the 180° preparation pulse of 800 ns duration has been applied. As discussed above, the ESE signal in this case consists of a narrow positive and a broad negative contributions. Trace 3 in Fig. 5 shows the ESE shape when an RF pulse with t_{rf} = 9 μs and θ_{rf} = 140° has been introduced between the preparation mw pulse and the detection sequence. One can see that the negative ESE component in trace 3 is considerably narrower than that in trace 2.

To analyze the EPR hole broadening quantitatively, we have used the procedure similar to that employed in (*24*). We have separated the negative contributions into the ESE signals by subtracting trace 1 from traces 2 and 3 in Fig. 5. The resulting ESE signals due to the EPR spectrum hole without and with the RF pulse are shown in Fig. 6 by traces 1 and 2, respectively. Dividing trace 2 by trace 1 in Fig. 6, we can obtain the Fourier image of the hole broadening function associated with the RF-induced nuclear spin inversion. It is shown by trace 3 in Fig. 6 upside down for the convenience of presentation.

It follows from Eq. [24] that the hole broadening and the corresponding ESE shape (trace 3 in Fig. 6) should be described by Gaussian functions. Indeed, a Gaussian function with a width $\Delta t \approx 390$ ns represents a very good fit to trace 3 in Fig. 6 (apart from the top of the signal where the residual narrow spike is still observable). The width of the local field distribution A_o in Eq. [24] is then equal to $2/(\pi\Delta t) \approx 1.63$ MHz. Substituting this value into Eq. [25] we obtain the density estimate $\rho \approx 0.028$ Å^{-3}, again in a qualitative agreement with the actual value of 0.037 Å^{-3}.

We have seen above that, in principle, a measurement of the ESE dependence on τ in Mims ENDOR and of an EPR hole width in Davies ENDOR enables us to estimate the density of matrix nuclei ρ in a sample. However, the estimates of ρ in a sample of a γ-irradiated malonic acid done in this work are about 20–25% lower than the actual density. The reason for this discrepancy is obviously related to the fact that our theoretical discussion was idealistic in some respects. First of all, the approximation about a uniform nuclear distribution might be not very good for relatively close nuclei (at the distances of the order of 10 Å) in a crystalline sample like the malonic acid powder. Besides, the lower limit of the integration over distances in Eq. [18]

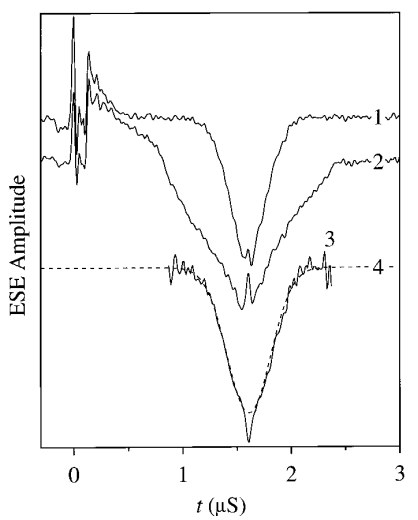

FIG. 6. Traces 1 and 2, the contributions of the EPR spectrum hole into the ESE signals in Fig. 5 obtained by subtraction of trace 1 in Fig. 5 from traces 3 and 2 in Fig. 5, respectively. Trace 3, a Fourier image of the hole-broadening function obtained by division of trace 1 by trace 2 (shown upside down for the convenience of presentation). Dashed trace 4, a Gaussian fit to trace 3 with a width between the maximum slope points of 390 ns.

should be greater than zero, about 2–4 Å (see (*16*) and the discussion above). For simplicity and because it was not of the primary importance, we have neglected this fact in our analysis, but it might be partly responsible for the underestimation of ρ. An important experimental factor that can lead to the underestimation of ρ is an inhomogeneity of the RF field in the resonator. For example, using the numerical calculations similar to those described above we can find that a Gaussian distribution of the RF field strength with a half-height width equal to the sample size will lead to the underestimation of ρ of the order of 15%. Any practical attempts to find an accurate estimate of ρ should take the above considerations into account. The purpose of this work, however, was to explain the matrix line phenomenon in principle rather than to obtain a perfect estimate of the proton density in the malonic acid.

In conclusion we may note that the analysis performed in this work shows that the finite intensity of the matrix line in the Mims and Davies ENDOR spectra is obtained due to the action of the RF pulse on a large number of the resonant nuclear spins. The fundamental reason for the matrix line effect is thus the same as that for the multiplet structure in the EPR spectra of the unpaired electrons interacting with many nuclei simultaneously, i.e., the additivity of the local magnetic fields produced by different nuclei at the position of the unpaired electron.

APPENDIX

Let us consider an ensemble of the unpaired electrons and magnetic nuclei coupled to them by a dipole interaction. The nuclei are assumed to be distributed in space with an average density ρ, but any nucleus is assumed to have an equal probability to occupy any position in space and thus the local nuclear densities at various coordinates may be different from ρ. Let the average number of nuclei coupled to an unpaired electron with a dipole interaction constant in the limits $D_k \pm \delta D_k$ be equal to $N_{k\pm}$. Then the probability of finding around an electron m nuclei satisfying a similar condition is obviously given by

$$p(m, N_{k\pm}) = [N!/m!(N - M)!] \cdot [N_{k\pm}/N]^m \times [1 - N_{k\pm}/N]^{N-m}, \quad [A1]$$

where $N \gg 1$ (and $N \gg m, N_{k\pm}$) is a total number of nuclei in the system. Substituting $N!$ and $(N - m)!$ by their Stirling expansions (e.g., $N! \approx (2\pi N)^{1/2} N^N \exp(-N)$) and taking into account that $N^{1/2}/(N - m)^{1/2} \approx 1$ we obtain

$$p(m, N_{k\pm}) = [N_{k\pm}^m (1 - N_{k\pm}/N)^{N-m} \exp(-m)]/[m!(1 - m/N)^{N-m}]. \quad [A2]$$

Finally, taking a limit at $N \to \infty$ results in

$$p(m, N_{k\pm}) \approx N_{k\pm}^m \exp(-N_{k\pm})/m!. \quad [A3]$$

This probability distribution peaks at $m = N_{k\pm}$ and has a half-height width of the order of $2N_{k\pm}^{1/2}$ for large $N_{k\pm}$.

We use Eq. [A3] in the numerical calculations of the matrix Mims ENDOR effect. A relatively small width of the distribution $p(m, N_{k\pm})$ excludes from consideration the values of m too strongly differing from $N_{k\pm}$. Therefore, the original (clearly not physical) assumption that any nucleus has an equal probability to occupy any position in space and thus any local nuclear density is allowed may not be considered as strictly prerequisite. Imposing physical restrictions on the local nuclear densities will limit a possible range of the m values. However, because several-fold variations of m in real systems are quite conceivable, Eq. [A3] is expected to hold to a good accuracy.

ACKNOWLEDGMENTS

A part of this work was supported by Hyogo Science and Technology Association (Japan). A.A. is grateful to Kwansei Gakuin University for inviting him as a guest professor. The authors are indebted to Dr. A. Raitsimring from the University of Arizona for stimulating discussions.

REFERENCES

1. W. B. Mims, *Proc. R. Soc. London* **283,** 482 (1965).
2. E. R. Davies, *Phys. Lett. A* **47,** 1 (1974).
3. P. F. Liao and S. R. Hartmann, *Phys. Rev. B* **8,** 69 (1973).
4. A. Stillman and R. N. Schwartz, *Molec. Phys.* **35,** 301 (1978).
5. K. P. Dinse, Pulsed ENDOR, *in* "Advanced EPR: Applications in Biology and Biochemistry" (A. J. Hoff, Ed.), p. 615, Elsevier, Amsterdam (1989).
6. C. Gemperle and A. Schweiger, *Chem. Rev.* **91,** 1481 (1991).
7. A. Grupp and M. Mehring, Pulsed ENDOR spectroscopy in solids, *in* "Modern Pulsed and Continuous Wave Electron Spin Resonance" (L. Kevan and M. Bowman, Eds.), p. 195, Wiley, New York (1990).
8. H. Thomann and M. Bernardo, Pulsed electron-nuclear double and multiple resonance spectroscopy of metals in proteins and enzymes, *in* "Biological Magnetic Resonance, EMR of Paramagnetic Molecules" (L. J. Berliner and J. Reuben, Eds.), Vol. 13, p. 275, Plenum, New York (1993).
9. R. P. J. Merks, R. de Beer, and D. van Ormondt, *Chem. Phys. Lett.* **61,** 142 (1979).
10. M. Hubrich, G. G. Maresch, and H. W. Spiess, *J. Magn. Reson. A* **113,** 177 (1995).
11. M. L. Gilchrist, J. A. Ball, D. W. Randall, and R. D. Britt, *Proc. Natl. Acad. Sci. USA* **92,** 9545 (1995).
12. H. Mino, A. V. Astashkin, and A. Kawamori, *Spectrochim. Acta A* **53,** 1465 (1997).
13. A. V. Astashkin, H. Mino, A. Kawamori, and T.-A. Ono, *Chem. Phys. Lett.* **272,** 506 (1997).
14. A. V. Astashkin, A. Kawamori, Y. Kodera, S. Kuroiwa, and K. Akabori, *J. Chem. Phys.* **102,** 5583 (1995).

15. P. E. Doan and B. M. Hoffman, *Chem. Phys. Lett.* **269,** 208 (1997).

16. S. A. Dikanov and Yu. D. Tsvetkov, "Electron Spin Echo Envelope Modulation (ESEEM) Spectroscopy," CRC Press, Boca Raton (1992).

17. A. Abragam, "The Principles of Nuclear Magnetism," Clarendon, Oxford (1961).

18. A. D. Milov, K. M. Salikhov, and M. D. Schirov, *Fiz. Tverd. Tela* **23,** 975 (1981).

19. V. V. Kurshev, A. M. Raitsimring, and Yu. D. Tsvetkov, *J. Magn. Reson.* **81,** 441 (1989).

20. A. Horsefield, J. R. Morton, and D. H. Whiffen, *Mol. Phys.* **4,** 327 (1961).

21. A. V. Astashkin and A. Schweiger, *Chem. Phys. Lett.* **174,** 595 (1990).

22. "Handbook of Chemistry and Physics" (R. C. Weast, Ed.), CRC Press, Cleveland (1975).

23. Th. Wacker, G. A. Sierra, and A. Schweiger, *Isr. J. Chem.* **32,** 305 (1992).

24. S. A. Dzuba, Y. Kodera, H. Hara, and A. Kawamori, *J. Magn. Reson. A* **102,** 257 (1993).